

Article

High-Performance CVD Bilayer MoS₂ Radio Frequency Transistors and Gigahertz Mixers for Flexible Nanoelectronics

Qingguo Gao ^{1,2} , Chongfu Zhang ^{1,2,*}, Kaiqiang Yang ¹, Xinjian Pan ¹, Zhi Zhang ¹, Jianjun Yang ¹, Zichuan Yi ¹, Feng Chi ¹ and Liming Liu ¹

¹ School of Electronic Information, University of Electronic Science and Technology of China, Zhongshan Institute, Zhongshan 528402, China; gqgemw@163.com (Q.G.); 201811022515@std.uestc.edu.cn (K.Y.); xinjianpan@163.com (X.P.); zz001@zsc.edu.cn (Z.Z.); sdyman@uestc.edu.cn (J.Y.); yizichuan@zsc.edu.cn (Z.Y.); chifeng@semi.ac.cn (F.C.); limingliu@uestc.edu.cn (L.L.)

² School of Information and Communication Engineering, University of Electronic Science and Technology of China, Chengdu 611731, China

* Correspondence: cfzhang@uestc.edu.cn

Abstract: Two-dimensional (2D) MoS₂ have attracted tremendous attention due to their potential applications in future flexible high-frequency electronics. Bilayer MoS₂ exhibits the advantages of carrier mobility when compared with monolayer mobility, thus making the former more suitable for use in future flexible high-frequency electronics. However, there are fewer systematical studies of chemical vapor deposition (CVD) bilayer MoS₂ radiofrequency (RF) transistors on flexible polyimide substrates. In this work, CVD bilayer MoS₂ RF transistors on flexible substrates with different gate lengths and gigahertz flexible frequency mixers were constructed and systematically studied. The extrinsic cutoff frequency (f_T) and maximum oscillation frequency (f_{max}) increased with reducing gate lengths. From transistors with a gate length of 0.3 μm , we demonstrated an extrinsic f_T of 4 GHz and f_{max} of 10 GHz. Furthermore, statistical analysis of 14 flexible MoS₂ RF transistors is presented in this work. The study of a flexible mixer demonstrates the dependence of conversion gain versus gate voltage, LO power and input signal frequency. These results present the potential of CVD bilayer MoS₂ for future flexible high-frequency electronics.

Keywords: bilayer MoS₂; CVD; high-frequency transistors; flexible electronics



Citation: Gao, Q.; Zhang, C.; Yang, K.; Pan, X.; Zhang, Z.; Yang, J.; Yi, Z.; Chi, F.; Liu, L. High-Performance CVD Bilayer MoS₂ Radio Frequency Transistors and Gigahertz Mixers for Flexible Nanoelectronics. *Micromachines* **2021**, *12*, 451. <https://doi.org/10.3390/mi12040451>

Academic Editors: Paulo M. Mendes and Bassem Jmai

Received: 27 March 2021

Accepted: 14 April 2021

Published: 16 April 2021

Publisher's Note: MDPI stays neutral with regard to jurisdictional claims in published maps and institutional affiliations.



Copyright: © 2021 by the authors. Licensee MDPI, Basel, Switzerland. This article is an open access article distributed under the terms and conditions of the Creative Commons Attribution (CC BY) license (<https://creativecommons.org/licenses/by/4.0/>).

1. Introduction

Owing to their ultimate thin thickness, superior mechanical flexibility and highly tunable electronic performance, two-dimensional materials for flexible applications have attracted tremendous attention [1–5]. Flexible transistors and devices based on 2D materials with high-speed are easy integrated with mature silicon CMOS manufacturing systems and can extend future flexible electronic systems even further with remote wireless capabilities. Recently, numerous devices and circuits using graphene, black phosphorous (BP) and molybdenum disulfide (MoS₂) were demonstrated for radio-frequency flexible electronics [6–13]. Graphene, which has an extraordinary carrier mobility of over 10,000 cm²/Vs and a high saturation velocity, has caused many researchers to realize high-performance flexible RF electronics with this extraordinary material. However, the current saturation of graphene transistors is poor due to the lack of bandgap of graphene [1,14]. Therefore, as a result, most graphene RF transistors may have a relatively lower f_{max} , which limits power gain at high frequency. On the other hand, BP has a sizeable bandgap and moderate carrier mobility (1000 cm²/Vs), which makes it suitable for both low-power and high-speed flexible devices [13,15,16]. However, its poor reliability and lack of large-area high-quality growth capabilities are still the key technological barriers in BP high-frequency electronics [17].

Unlike graphene and BP, two-dimensional MoS₂ with long-term air stability has a sizable bandgap, relative moderate carrier mobility and saturation velocity, and large-area growth capability. As an atomically thin semiconductor, 2D MoS₂ have demonstrated great potential for use in high-frequency electronics, next-generation logic circuits and flexible electronics [9,18–22]. In 2014, radio-frequency transistors fabricated using exfoliated MoS₂ demonstrated an extrinsic f_T of 2.1 GHz and f_{max} of 8 GHz on rigid Si/SiO₂ substrates [22]. In the same year, exfoliated few-layer MoS₂ RF transistors with self-aligned gates on rigid quartz and flexible polyimide substrates were reported [9]. The frequency responses of the self-aligned transistors on rigid quartz substrate showed an extrinsic f_T of 10.2 GHz and f_{max} of 14.5 GHz; a gigahertz inverter and amplifier were also demonstrated. Additionally, the frequency response of the self-aligned transistors on flexible PI substrate shown an extrinsic f_T and f_{max} of 4.7 and 5.4 GHz, respectively. Recently, Zhang et al. presented an flexible rectenna based on MoS₂ high-frequency diodes with a cutoff frequency of 10 GHz [18]. Although these works have demonstrated the potential of high-frequency MoS₂ devices, exfoliated MoS₂ lack precise control of flake size and thickness, which hamper large-scale commercial manufacturing and applications [23,24].

Chemical vapor deposition (CVD) is a low-cost and important method to produce large-area, high-quality MoS₂ film. High-quality uniform CVD monolayer MoS₂ film larger than two inches has been growth by different groups [4,23–25]. In 2015, RF transistors based on CVD monolayer MoS₂ with an extrinsic f_T of 2.8 GHz and f_{max} of 3.6 GHz were reported, and simple circuit demos, such as the megahertz MoS₂ frequency mixer and common-source amplifier, were also demonstrated [26]. As has been done with exfoliated MoS₂, optimized gate configuration was applied to CVD MoS₂ transistors to achieve higher cut-off frequencies [27]. With optimized embedded gate structure, CVD monolayer MoS₂ transistors with improved extrinsic f_T of 3.3 GHz and f_{max} of 9.8 GHz were fabricated. Although the RF performance of CVD MoS₂ transistors was advanced with optimized device configuration, neither f_T nor f_{max} can reach the level of exfoliated MoS₂ transistors, which severely limits their high-frequency applications. Bilayer MoS₂ usually has higher carrier mobility and higher density of states, which in turn will result in superior performance over electronic devices based on monolayers [28–30]. In 2018, CVD bilayer MoS₂ RF transistors with extrinsic f_T of 7.2 GHz and f_{max} of 23 GHz were demonstrated. For flexible high frequency transistors, extrinsic f_T and f_{max} of 2.7 and 2.1 GHz were obtained based on CVD monolayer MoS₂ [11], and the extrinsic f_T and f_{max} of 4 and 9 GHz were obtained based on CVD bilayer MoS₂ [31]. Although flexible MoS₂ RF transistors based on CVD bilayer MoS₂ have been demonstrated, there still many problems that need to be investigated. The reported flexible CVD bilayer MoS₂ RF transistors only have one gate length. Its scaling behavior is still unexplored. Additionally, statistical analysis of MoS₂ flexible RF transistors with different gate lengths needs more research, which is important to understand the uniformity of MoS₂ RF transistors and helpful to acquire deep insight into the limited factor of large-scale high performance MoS₂ RF transistors [32].

In this work, a systematic study of CVD bilayer MoS₂ RF transistors on flexible substrates is presented. First, high-quality chemical vapor deposited bilayer MoS₂ were grown on molten glass and transferred onto a Si₃N₄/PI substrate. The fabrication process of flexible high-frequency MoS₂ transistors was presented. An extrinsic field-effect mobility of 5 cm²/Vs and a high I_{on}/I_{off} ratio of 10⁸ were demonstrated with flexible bilayer MoS₂ transistors. High-frequency measurements up to 10 GHz and statistical analysis were carried out for 14 MoS₂ RF transistors with gate lengths of 0.3 μm, 0.6 μm, and 1 μm. Cut-off frequency and maximum oscillation frequency increased as the gate length was scaled down. Extrinsic f_T of 4 GHz and f_{max} of 10 GHz were achieved for the 0.3 μm transistors. Additionally, the transistors with larger gate length had better high-frequency performance uniformity. Finally, conversion gain of gigahertz MoS₂ frequency mixer versus gate voltage, frequency and input power were systematically investigated.

2. Materials and Methods

2.1. Material Growth and Characterization

The bilayer MoS₂ films were grown on molten glass substrates using sulfur powders and MoO₃ powders as reaction precursors in a two-zone furnace. Then, an alumina crucible with 1.4 g sulfur powder and a quartz crucible with 2 mg MoO₃ precursor and glass substrates were placed at the center of first and second heating zones, respectively. The distance between the MoO₃ precursor and glass substrates was about 2 mm. The temperatures of the first and second zones were ramped to 230 °C and 830 °C, respectively. During the ramping and growth process, a 40 sccm Ar flow was introduced as the carrier gas, and the pressure within the quartz tube was controlled to 1 atm pressure. After a growth duration of 10 min, the furnace was turned off, and the system began to cool down. Figure 1a shows a typical optical microscopy of the bilayer; MoS₂ with a triangular shape shows a highly uniform color contrast in the bilayer region, indicating homogenous thickness. The thickness and quality of the CVD bilayer MoS₂ were then characterized by an atomic force microscope (AFM), Raman spectroscopy and photoluminescence analyses. Figure 1b shows the AFM image of the edge of the bilayer MoS₂, and the corresponding height profile presents a thickness of 1.34 nm [33]. As shown in Figure 1c, after being transferred onto SiO₂/Si substrates, the bilayer MoS₂ shows typical Raman spectra with an E¹_{2g} peak of 385.7 cm⁻¹ and A_{1g} peak of 408.3 cm⁻¹. The delta value between the E¹_{2g} and A_{1g} peaks is 22.6 cm⁻¹, which is consistent with previous reports of bilayer MoS₂ [34–36]. The typical photoluminescence (PL) spectrum of the bilayer MoS₂ is shown in Figure 1d, where the peaks at around 665 and 618 nm correspond to the A1 and B1 direct excitonic transitions at 1.86 and 2.01 eV, respectively [31,37]. What's more, as shown in Figure S1, further elemental analysis of the CVD-grown MoS₂ was studied by X-ray photoelectron spectroscopy (XPS). More details about material characterizations of CVD-grown MoS₂ can be found in our previous works [31].

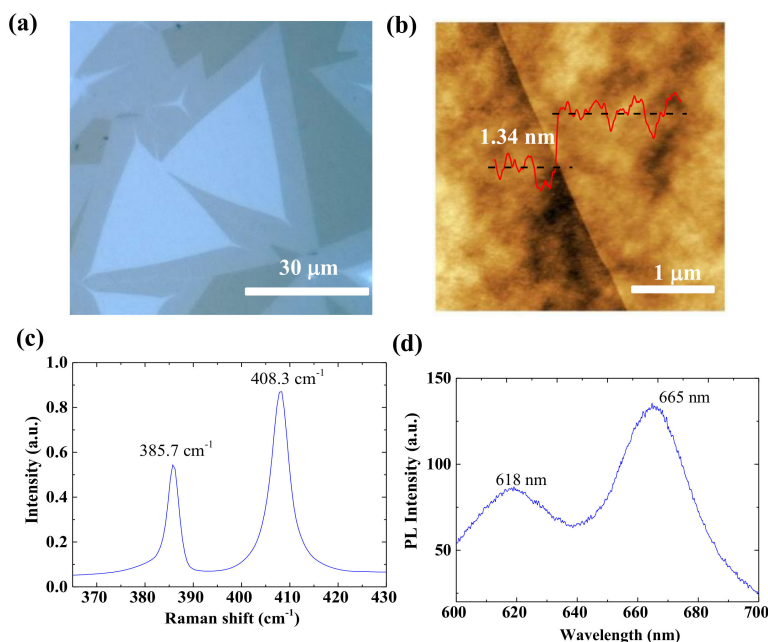


Figure 1. (a) Optical micrograph of chemical vapor deposition (CVD) bilayer MoS₂ on molten glass. (b) Atomic force microscopy image of bilayer MoS₂ on SiO₂/Si substrates after transfer. Raman (c) and photoluminescence (PL) spectra (d) of high-quality CVD bilayer MoS₂.

2.2. Device Fabrication

Figure 2 shows the fabrication process flows and device schematic of the bilayer MoS₂ RF devices on flexible polyimide substrates. Prior to fabrication, the commercially available PI substrates (Dupont Kapton 500HN) were cleaned in acetone, isopropyl alcohol (IPA)

and deionized water. To reduce the surface roughness, 100 nm of Si_3N_4 were deposited by plasma-enhanced CVD (PECVD). Then, bilayer MoS_2 films were transferred onto polyimide substrates via the polymethyl methacrylate (PMMA)-assisted transfer method [23,25]. Different from conventional acidic or alkaline solutions as etchant, deionized water was utilized here for the hydrophobicity/hydrophilicity property of the as-grown MoS_2 /glass stack. As shown in Figure 3a, the high-quality triangle shape of bilayer MoS_2 was well preserved, which is important for the fabrication of high-performance MoS_2 transistors. After the transfer process, bilayer MoS_2 films were patterned with an electron beam lithography (EBL) step and etched using O_2/Ar plasma. Source and drain contact electrodes were formed by electron beam evaporation (EBE) with 20/60-nm Ni/Au metal stacks. To form a uniform top-gate dielectric, 2-nm Al was grown by EBE as a seed layer before the atomic layer deposition (ALD) of HfO_2 . Finally, the two-fingers top-gate electrode of 20/60-nm Ni/Au was defined by EBL and deposited by EBE. The high-frequency bilayer MoS_2 transistors on flexible PI substrates after fabrication are shown in Figure 3b,c. In this work, the MoS_2 RF transistors are designed with different gate lengths of 0.3 μm , 0.6 μm , and 1 μm and the same gate width of $2 \times 15 \mu\text{m}$. Figure 3d shows an optical microscope of a device with a gate length of 1 μm , exhibiting the precise alignment of the gate structure to the source/drain area. From the theory of high-frequency electronics, both gate to drain/source capacitance $C_{\text{gd}}/C_{\text{gs}}$ and series resistance are critical factors in high-performance RF transistors. In this device design, there is no overlap between gate and source/drain electrodes to avoid excess C_{gd} and C_{gs} . Additionally, the gate to source/drain access lengths L_{gs} and L_{gd} are minimized to decrease the series resistance.

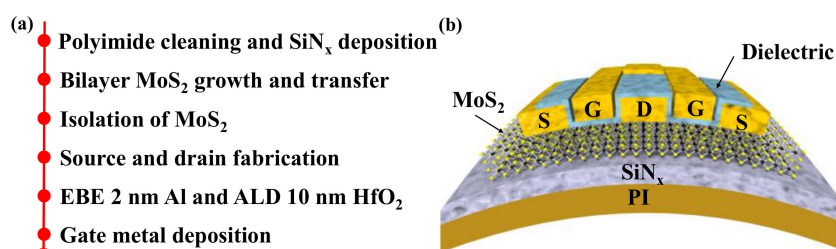


Figure 2. (a) Process flows and (b) schematic cross-section of the fabricated flexible bilayer MoS_2 RF transistors.

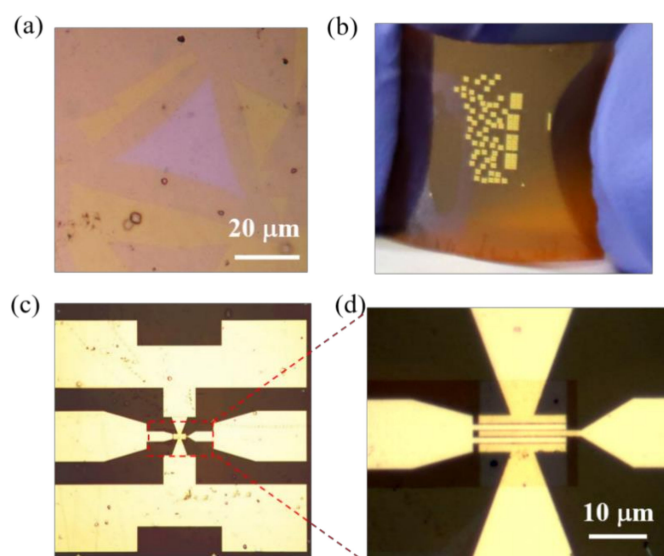


Figure 3. (a) The transferred bilayer MoS_2 on polyimide substrates. (b) Optical images of the fabricated flexible MoS_2 RF transistors. (c,d) Optical images of the flexible MoS_2 RF transistor with ground-signal-ground (GSG) structure showing excellent alignment.

3. Results and Discussion

3.1. DC Characterization

Figure 4a,b shows the measured transfer and output characteristics of CVD bilayer MoS₂ transistors on polyimide substrates. A high I_{on}/I_{off} ratio of 10^8 is achieved, making these devices ideal for ultra-low power applications. The extrinsic low-field effect mobility of $5 \text{ cm}^2/\text{Vs}$ is extracted. Here, we note that the extracted mobility value is underestimated as there is a non-negligible contact resistance contribution to the total device resistance. The intrinsic mobility of our bilayer MoS₂ on rigid substrates is calculated to be $36 \text{ cm}^2/\text{Vs}$ [31]. The degradation of mobility can be attributed to the increased surface roughness and poor thermal conductivity of organic flexible substrates. The output characteristics of bilayer MoS₂ transistors on polyimide shows applicable current saturation. An on-current density of $30 \text{ } \mu\text{A}/\mu\text{m}$ was demonstrated with the $L_g = 1 \text{ } \mu\text{m}$ device. For comparison, we also fabricated flexible monolayer MoS₂ transistors on polyimide substrates. An extrinsic carrier mobility of $0.2 \text{ cm}^2/\text{Vs}$ and an on-current density of $1.2 \text{ } \mu\text{A}/\mu\text{m}$ were obtained with the same gate length, showing the superiority of CVD bilayer MoS₂ for flexible electronic applications.

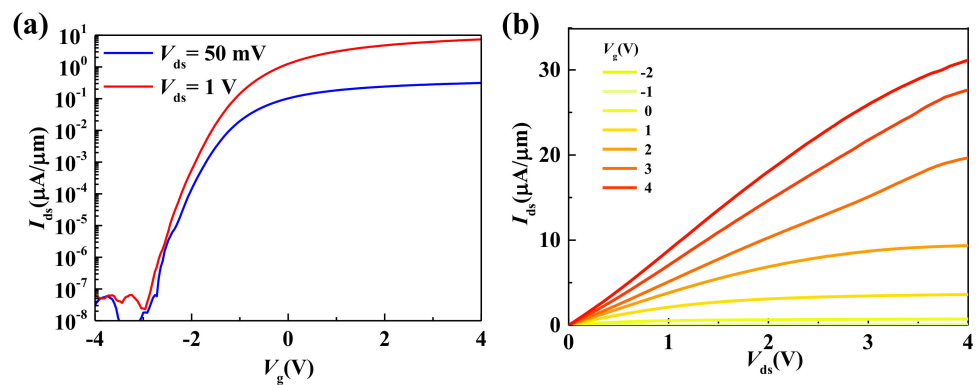


Figure 4. (a) Transfer characteristics at $V_{ds} = 50 \text{ mV}$ and 1 V . I_{on}/I_{off} ratio are about 10^8 , making these devices ideal for ultra-low power applications. (b) Output characteristics of flexible CVD bilayer MoS₂ transistors at various V_g .

3.2. RF Characterization

Cutoff frequency f_T and maximum oscillation frequency f_{max} are commonly used to characterize the high-frequency performance of RF transistors. f_T corresponds to the frequency where the short-circuit current gain becomes unity. From the small signal equivalent circuit of the transistor, f_T can be described using

$$f_T = \frac{g_m}{2\pi} * \frac{1}{(C_{gs} + C_{gd})[1 + g_{ds}(R_s + R_d)] + C_{gd}g_m(R_s + R_d)} \quad (1)$$

where C_{gs} is the gate to source capacitance, C_{gd} is the gate to drain capacitance, g_m is the transconductance, g_{ds} is the output conductance, and R_s and R_d are the source and drain series resistances, respectively. f_{max} correspond to the frequency where the unilateral power gain becomes unity. f_{max} can be described using

$$f_{max} = \frac{f_T}{2\sqrt{g_{ds}(R_s + R_d) + 2\pi f_T C_g R_g}} \quad (2)$$

where R_g is the gate resistance, which can be reduced through the increase of gate metal area and thickness. To evaluate the high-frequency performance of the CVD bilayer MoS₂ transistors, standard on-chip S-parameter measurements up to 10 GHz were performed. Figure 5a,b show the as-measured extrinsic small-signal current gain ($|h_{21}|$) and Mason's unilateral power gain (U) as a function of frequency for the CVD bilayer

MoS₂ transistors. An extrinsic f_T of 4 GHz and f_{max} of 10 GHz were achieved where, as shown in Table 1, the f_{max} is the highest extrinsic maximum oscillation frequency among flexible MoS₂ RF transistors [9,11], demonstrating the potential of bilayer MoS₂ for large-scale, high-performance RF applications. What's more, f_{max} is also comparable to MoS₂ transistors on rigid substrates with the same gate length [31]. This can be attributed to the decreased high-frequency parasitic effect in insulating polyimide substrates, although the roughness and poor thermal conductivity of polyimide substrates degrade the DC transport performance of the MoS₂ transistors [12].

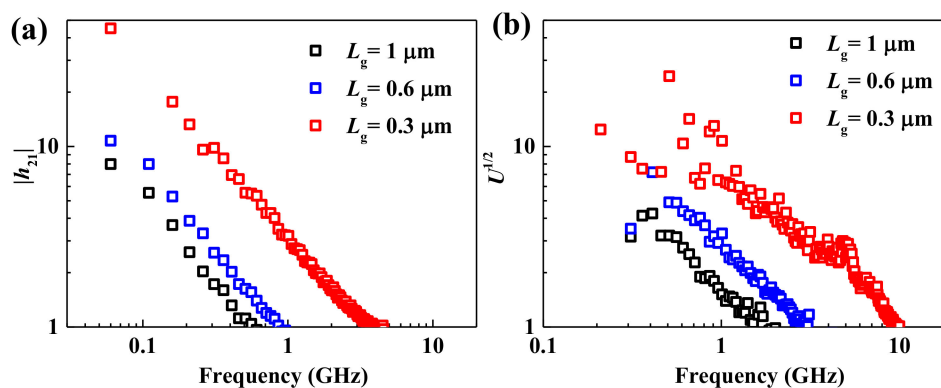


Figure 5. (a) Small-signal current gain $|h_{21}|$ versus frequency of flexible MoS₂ transistors with gate lengths of 0.3 μm , 0.6 μm , and 1 μm . (b) The corresponding unilateral power gain versus frequency.

Table 1. Comparison of flexible high-frequency transistors based on 2D MoS₂.

MoS ₂	Substrate	L_g (nm)	$f_{T,\text{extrinsic}}$ (GHz)	$f_{\text{max,extrinsic}}$ (GHz)	References
Exfoliated	PI	68	4.7	5.4	[9]
CVD	PI	500	2.7	2.1	[11]
CVD	PI	300	4	9	[31]
CVD	PI	300	4	10	This Work

Figure 6, displaying the devices' data, gives some insight into the statistical analysis and scalability of CVD bilayer MoS₂ RF transistors on flexible PI substrates. The extrinsic f_T and f_{max} of 14 MoS₂ devices with different gate lengths are plotted in Figure 6a,b, respectively. Both f_T and f_{max} increase as the gate length decreases. Additionally, through gate length scaling down, it is possible to further improve the f_T and f_{max} . Variations of f_T and f_{max} within devices of the same gate length can be observed, especially for transistors with a gate length of 0.3 μm . Here, we attribute these variations to the varied alignment of gate and source/drain electrodes in the EBL process of short gate length transistors. Since flexible organic substrates are not conductive and easily result in deformation, not all devices in this work could realize the perfect alignment of gate and source/drain electrodes, as shown in Figure 3d. Short gate length RF transistors are more prone to uniformity problems. Therefore, the contact resistance, substrate roughness and fabrication process are still critical limitations of flexible bilayer MoS₂ RF transistors. It should be pointed out that MoS₂ transistors with 1T phase electrodes exhibiting contact resistance of 200–300 $\Omega \cdot \mu\text{m}$ have been demonstrated [38]. MoS₂ polymorphs with diverse electrical properties and their applications in high-frequency nanoelectronics are fascinating [18,38–43] and require further investigation.

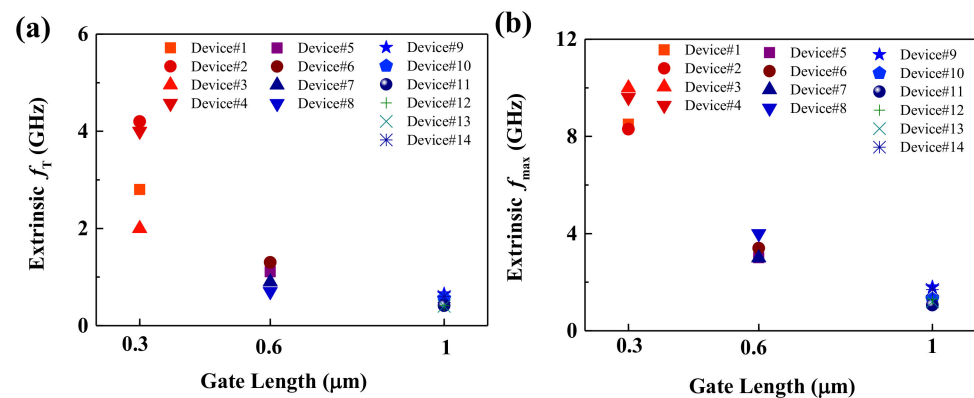


Figure 6. Extrinsic f_T and f_{max} of 14 flexible MoS₂ RF transistors. (a) Extrinsic f_T as a function of gate length. (b) Extrinsic f_{max} as a function of gate length.

Although flexible MoS₂ mixers have been demonstrated in previous work [11,31], the frequency response and gate bias voltage dependence of flexible MoS₂ mixers have not been reported. In this work, active mixers based on flexible bilayer MoS₂ transistors were demonstrated and systematically researched. Mixer measurements were carried out at room temperature with an RF input frequency of 1.5 GHz and local oscillation (LO) frequency of 1.4 GHz. Figure 7a shows the measured IF output signal (0.1 MHz) using a signal analyzer. The conversion gain versus the input frequency is plotted in Figure 7b. When the input signal powers and f_{IF} of 100 MHz are the same, conversion gain decreases as frequency increase from 0.8 to 1.9 GHz. Figure 7c shows the conversion gain versus LO power. A conversion gain of -52.3 dB could be achieved with f_{RF} of 1.5 GHz. For the flexible active MoS₂ mixer, as shown in Figure 7d, gate bias voltage is important to achieve the maximum conversion gain. This is because DC transconductance, the same as cutoff frequency and maximum oscillation frequency, has a strong dependence on gate bias voltage.

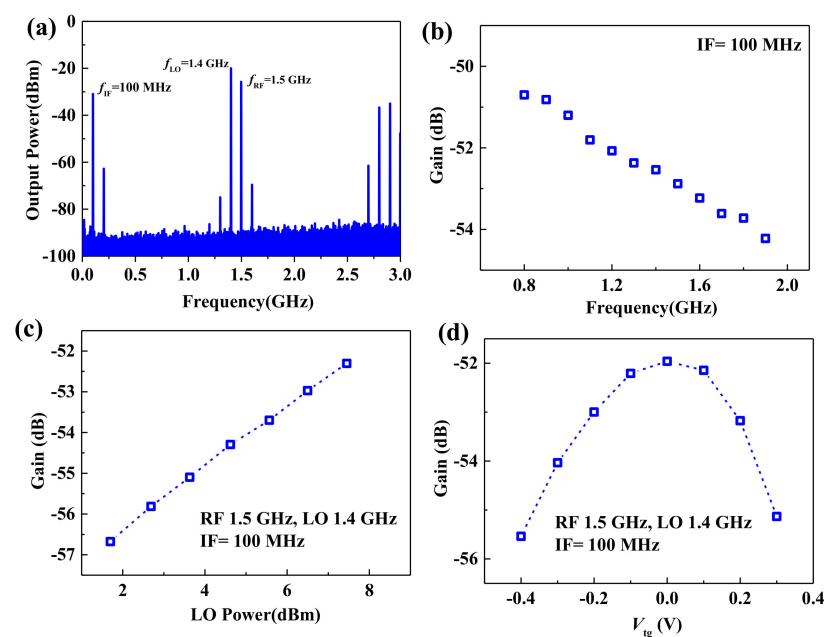


Figure 7. Gigahertz flexible MoS₂ mixer. (a) Output frequency spectrum of the flexible MoS₂ mixer. (b) Conversion gain of MoS₂ mixer versus input frequency. (c) Conversion gain of MoS₂ mixer versus local oscillation (LO) power. (d) Conversion gain of MoS₂ mixer versus gate voltage.

4. Conclusions

In this work, we constructed high-frequency transistors and gigahertz mixers on flexible polyimide substrates based on CVD bilayer MoS₂, and their high-frequency performance was systematically assessed. Record extrinsic f_{\max} as high as 10 GHz have been demonstrated with 0.3 μm devices. The scaling behavior of MoS₂ RF transistors on flexible polyimide substrates was studied, and the extrinsic f_T and f_{\max} were increased as gate length decreased, showing the potential for further improvement through decreasing the gate lengths. Statistical analysis of 14 flexible MoS₂ RF transistors with different gate length showed RF performance variation in short gate length MoS₂ transistors. We systematically studied the dependence of flexible MoS₂ mixer conversion gain on gate bias voltage, f_{RF} and LO power, addressing the importance of V_{tg} , LO power and f_{RF} on high-performance flexible MoS₂ mixers. Our results advance the achieved maximum oscillation frequency of flexible CVD MoS₂ transistors and represent a step towards high-performance flexible MoS₂ wireless communications systems.

Supplementary Materials: The following are available online at <https://www.mdpi.com/article/10.3390/mi12040451/s1>, Figure S1: (a) The XPS spectra of the Mo 3d state, (b) S 2s state.

Author Contributions: Conceptualization, Q.G. and C.Z.; methodology, Q.G., K.Y. and X.P.; validation, Q.G. and Z.Z.; formal analysis, Q.G., Z.Z. and X.P.; investigation, Q.G.; resources, C.Z., Z.Y., J.Y., F.C. and L.L.; data curation, Q.G.; writing—original draft preparation, Q.G. and C.Z.; writing—review and editing, Q.G. and C.Z.; visualization, Q.G.; supervision, Q.G. and C.Z.; project administration, Q.G. and C.Z.; funding acquisition, Q.G., Z.Y. and C.Z. All authors have read and agreed to the published version of the manuscript.

Funding: This work was funded in part by the Guangdong Basic and Applied Basic Research Foundation (Grant No. 2019A1515110752), in part by the Youth Innovative Talent Project of Guangdong Education Department (Grant No. 2019KQNCX187), in part by the Outstanding Chinese and Foreign Youth Exchange Program of China Association for Science and Technology (CAST), 2019, in part by the Natural Science Foundation of China (Grant No. 62071088), and in part by the Project for Innovation Team of Guangdong University (Grant No. 2018KCXTD033), in part by National Key R&D Program of China (Grant No. 2018YFB1801302), in part by Zhongshan Social Public Welfare Science and Technology (Grant No. 2019B2007), in part by Research Project for Talent of UESTC Zhongshan Institute (419YKQN09).

Data Availability Statement: The data that support the findings of this study are available from the corresponding author upon reasonable request.

Conflicts of Interest: The authors declare no conflict of interest.

References

1. Akinwande, D.; Huyghebaert, C.; Wang, C.-H.; Serna, M.I.; Goossens, S.; Li, L.-J.; Wong, H.-S.P.; Koppens, F.H.L. Graphene and two-dimensional materials for silicon technology. *Nat. Cell Biol.* **2019**, *573*, 507–518. [[CrossRef](#)]
2. Li, C.; Xiong, K.; Li, L.; Guo, Q.; Chen, X.; Madjar, A.; Watanabe, K.; Taniguchi, T.; Hwang, J.C.M.; Xia, F. Black Phosphorus High-Frequency Transistors with Local Contact Bias. *ACS Nano* **2020**, *14*, 2118–2125. [[CrossRef](#)]
3. Xiong, X.; Huang, M.; Hu, B.; Li, X.; Liu, F.; Li, S.; Tian, M.; Li, T.; Song, J.; Wu, Y. A transverse tunnelling field-effect transistor made from a van der Waals heterostructure. *Nat. Electron.* **2020**, *3*, 106–112. [[CrossRef](#)]
4. Yang, P.; Zhang, S.; Pan, S.; Tang, B.; Liang, Y.; Zhao, X.; Zhang, Z.; Shi, J.; Huan, Y.; Shi, Y.; et al. Epitaxial Growth of Centimeter-Scale Single-Crystal MoS₂ Monolayer on Au(111). *ACS Nano* **2020**, *14*, 5036–5045. [[CrossRef](#)] [[PubMed](#)]
5. Gao, Q.; Li, X.; Tian, M.; Xiong, X.; Zhang, Z.; Wu, Y. Short-Channel Graphene Mixer with High Linearity. *IEEE Electron. Device Lett.* **2017**, *38*, 1168–1171. [[CrossRef](#)]
6. Pu, J.; Yomogida, Y.; Liu, K.-K.; Li, L.-J.; Iwasa, Y.; Takenobu, T. Highly flexible MoS₂ thin-film transistors with ion gel dielectrics. *Nano Lett.* **2012**, *12*, 4013–4017. [[CrossRef](#)] [[PubMed](#)]
7. Chang, H.-Y.; Yang, S.; Lee, J.; Tao, L.; Hwang, W.-S.; Jena, D.; Lu, N.; Akinwande, D. High-Performance, Highly Bendable MoS₂ Transistors with High-K Dielectrics for Flexible Low-Power Systems. *ACS Nano* **2013**, *7*, 5446–5452. [[CrossRef](#)] [[PubMed](#)]
8. Akinwande, D.; Petrone, N.; Hone, J. Two-dimensional flexible nanoelectronics. *Nat. Commun.* **2014**, *5*, 5678. [[CrossRef](#)] [[PubMed](#)]
9. Cheng, R.; Jiang, S.; Chen, Y.; Liu, Y.; Weiss, N.; Cheng, H.-C.; Wu, H.; Huang, Y.; Duan, X. Few-layer molybdenum disulfide transistors and circuits for high-speed flexible electronics. *Nat. Commun.* **2014**, *5*, 5143. [[CrossRef](#)]

10. Park, J.; Choudhary, N.; Smith, J.; Lee, G.; Kim, M.; Choi, W. Thickness modulated MoS₂ grown by chemical vapor deposition for transparent and flexible electronic devices. *Appl. Phys. Lett.* **2015**, *106*, 012104. [[CrossRef](#)]
11. Chang, H.-Y.; Yogeesh, M.N.; Ghosh, R.; Rai, A.; Sanne, A.; Yang, S.; Lu, N.; Banerjee, S.K.; Akinwande, D. Large-Area Monolayer MoS₂ for Flexible Low-Power RF Nanoelectronics in the GHz Regime. *Adv. Mater.* **2016**, *28*, 1818–1823. [[CrossRef](#)]
12. Park, S.; Shin, S.H.; Yogeesh, M.N.; Lee, A.L.; Rahimi, S.; Akinwande, D. Extremely High-Frequency Flexible Graphene Thin-Film Transistors. *IEEE Electron. Device Lett.* **2016**, *37*, 512–515. [[CrossRef](#)]
13. Zhu, W.; Park, S.; Yogeesh, M.N.; McNicholas, K.M.; Bank, S.R.; Akinwande, D. Black phosphorus flexible thin film transistors at gighertz frequencies. *Nano Lett.* **2016**, *16*, 2301–2306. [[CrossRef](#)] [[PubMed](#)]
14. Wu, Y.; Lin, Y.-M.; Bol, A.A.; Jenkins, K.A.; Xia, F.; Farmer, D.B.; Zhu, Y.; Avouris, P. High-frequency, scaled graphene transistors on diamond-like carbon. *Nature* **2011**, *472*, 74–78. [[CrossRef](#)]
15. Liu, H.; Neal, A.T.; Zhu, Z.; Luo, Z.; Xu, X.; Tománek, D.; Ye, P.D. Phosphorene: An Unexplored 2D Semiconductor with a High Hole Mobility. *ACS Nano* **2014**, *8*, 4033–4041. [[CrossRef](#)] [[PubMed](#)]
16. Wang, H.; Wang, X.; Xia, F.; Wang, L.; Jiang, H.; Xia, Q.; Chin, M.L.; Dubey, M.; Han, S.-J. Black phosphorus radio-frequency transistors. *Nano Lett.* **2014**, *14*, 6424–6429. [[CrossRef](#)] [[PubMed](#)]
17. Wan, D.; Huang, H.; Wang, Z.; Liu, X.; Liao, L. Recent advances in long-term stable black phosphorus transistors. *Nanoscale* **2020**, *12*, 20089–20099. [[CrossRef](#)] [[PubMed](#)]
18. Zhang, X.; Grajal, J.; Vazquez-Roy, J.L.; Radhakrishna, U.; Wang, X.; Chern, W.; Zhou, L.; Lin, Y.; Shen, P.-C.; Ji, X.; et al. Two-dimensional MoS₂-enabled flexible rectenna for Wi-Fi-band wireless energy harvesting. *Nat. Cell Biol.* **2019**, *566*, 368–372. [[CrossRef](#)]
19. Lin, Z.; Liu, Y.; Halim, U.; Ding, M.; Liu, Y.; Wang, Y.; Jia, C.; Chen, P.; Duan, X.; Wang, C.; et al. Solution-processable 2D semiconductors for high-performance large-area electronics. *Nat. Cell Biol.* **2018**, *562*, 254–258. [[CrossRef](#)]
20. Desai, S.B.; Madhvapathy, S.R.; Sachid, A.B.; Llinas, J.P.; Wang, Q.; Ahn, G.H.; Pitner, G.; Kim, M.J.; Bokor, J.; Hu, C.; et al. MoS₂ transistors with 1-nanometer gate lengths. *Science* **2016**, *354*, 99–102. [[CrossRef](#)]
21. Tasker, P.J.; Hughes, B. Importance of source and drain resistance to the maximum f_T of millimeter-wave MODFETs. *IEEE Electron. Device Lett.* **1989**, *10*, 291–293. [[CrossRef](#)]
22. Krasnozhan, D.; Lembke, D.; Nyffeler, C.; Leblebici, Y.; Kis, A. MoS₂ Transistors Operating at Gigahertz Frequencies. *Nano Lett.* **2014**, *14*, 5905–5911. [[CrossRef](#)] [[PubMed](#)]
23. Wang, Q.; Li, N.; Tang, J.; Zhu, J.; Zhang, Q.; Jia, Q.; Lu, Y.; Wei, Z.; Yu, H.; Zhao, Y.; et al. Wafer-Scale Highly Oriented Monolayer MoS₂ with Large Domain Sizes. *Nano Lett.* **2020**, *20*, 7193–7199. [[CrossRef](#)] [[PubMed](#)]
24. Guangyu, Z.; Liao, M.; Zhao, W.; Liu, G.; Zhou, X.J.; Wei, Z.; Xu, X.; Liu, K.; Hu, Z.; Deng, K.; et al. Wafer-Scale Growth and Transfer of Highly-Oriented Monolayer MoS₂ Continuous Films. *ACS Nano* **2017**, *11*, 12001–12007. [[CrossRef](#)]
25. Yang, P.; Zou, X.; Zhang, Z.; Zhongfan, L.; Shi, J.; Chen, S.; Shulin, C.; Zhao, L.; Jiang, S.; Zhou, X.; et al. Batch production of 6-inch uniform monolayer molybdenum disulfide catalyzed by sodium in glass. *Nat. Commun.* **2018**, *9*, 1–10. [[CrossRef](#)]
26. Sanne, A.; Ghosh, R.; Rai, A.; Yogeesh, M.N.; Shin, S.H.; Sharma, A.; Jarvis, K.; Mathew, L.; Rao, R.; Akinwande, D.; et al. Radio Frequency Transistors and Circuits Based on CVD MoS. *Nano Lett.* **2015**, *15*, 5039–5045. [[CrossRef](#)] [[PubMed](#)]
27. Sanne, A.; Park, S.; Ghosh, R.; Yogeesh, M.N.; Liu, C.; Mathew, L.; Rao, R.; Akinwande, D.; Banerjee, S.K. Embedded gate CVD MoS₂ microwave FETs. *NPJ 2D Mater. Appl.* **2017**, *1*, 26. [[CrossRef](#)]
28. Wang, X.; Feng, H.; Wu, Y.; Jiao, L. Controlled Synthesis of Highly Crystalline MoS₂ Flakes by Chemical Vapor Deposition. *J. Am. Chem. Soc.* **2013**, *135*, 5304–5307. [[CrossRef](#)]
29. Zobel, A.; Bosen, A.; Wilson, P.M.; Muratov, D.S.; Kuznetsov, D.V.; Sinitiskii, A. Chemical vapour deposition and characterization of uniform bilayer and trilayer MoS₂ crystals. *J. Mater. Chem. C* **2016**, *4*, 11081–11087. [[CrossRef](#)]
30. Jeon, J.; Jang, S.K.; Jeon, S.M.; Yoo, G.; Jang, Y.H.; Park, J.-H.; Lee, S. Layer-controlled CVD growth of large-area two-dimensional MoS₂films. *Nanoscale* **2015**, *7*, 1688–1695. [[CrossRef](#)]
31. Gao, Q.; Zhang, Z.; Xu, X.; Song, J.; Li, X.; Wu, Y. Scalable high performance radio frequency electronics based on large domain bilayer MoS₂. *Nat. Commun.* **2018**, *9*, 4778. [[CrossRef](#)] [[PubMed](#)]
32. Tian, M.; Hu, B.; Yang, H.; Tang, C.; Wang, M.; Gao, Q.; Xiong, X.; Zhang, Z.; Li, T.; Li, X.; et al. Wafer Scale Mapping and Statistical Analysis of Radio Frequency Characteristics in Highly Uniform CVD Graphene Transistors. *Adv. Electron. Mater.* **2019**, *5*, 1800711. [[CrossRef](#)]
33. Wang, H.; Yu, L.; Lee, Y.-H.; Shi, Y.; Hsu, A.; Chin, M.L.; Li, L.-J.; Dubey, M.; Kong, J.; Palacios, T. Integrated Circuits Based on Bilayer MoS₂ Transistors. *Nano Lett.* **2012**, *12*, 4674–4680. [[CrossRef](#)]
34. Chang, M.-C.; Ho, P.-H.; Tseng, M.-F.; Lin, F.-Y.; Hou, C.-H.; Lin, I.-K.; Wang, H.; Huang, P.-P.; Chiang, C.-H.; Yang, Y.-C.; et al. Fast growth of large-grain and continuous MoS₂ films through a self-capping vapor-liquid-solid method. *Nat. Commun.* **2020**, *11*, 1–9. [[CrossRef](#)] [[PubMed](#)]
35. Zhang, X.; Nan, H.; Xiao, S.; Wan, X.; Gu, X.; Du, A.; Ni, Z.; Ostrikov, K.K. Transition metal dichalcogenides bilayer single crystals by reverse-flow chemical vapor epitaxy. *Nat. Commun.* **2019**, *10*, 1–10. [[CrossRef](#)]
36. Li, H.; Zhang, Q.; Yap, C.C.R.; Tay, B.K.; Edwin, T.H.T.; Olivier, A.; Baillargeat, D. From Bulk to Monolayer MoS₂: Evolution of Raman Scattering. *Adv. Funct. Mater.* **2012**, *22*, 1385–1390. [[CrossRef](#)]
37. Splendiani, A.; Sun, L.; Zhang, Y.; Li, T.; Kim, J.; Chim, C.-Y.; Galli, G.; Wang, F. Emerging Photoluminescence in Monolayer MoS. *Nano Lett.* **2010**, *10*, 1271–1275. [[CrossRef](#)]

38. Kappera, R.; Voiry, D.; Yalcin, S.E.; Branch, B.; Gupta, G.; Mohite, A.D.; Chhowalla, M. Phase-engineered low-resistance contacts for ultrathin MoS₂ transistors. *Nat. Mater.* **2014**, *13*, 1128–1134. [[CrossRef](#)]
39. Kim, J.S.; Kim, J.; Zhao, J.; Kim, S.; Lee, J.H.; Jin, Y.; Choi, H.; Moon, B.H.; Bae, J.J.; Lee, Y.H.; et al. Electrical Transport Properties of Polymorphic MoS. *ACS Nano* **2016**, *10*, 7500–7506. [[CrossRef](#)]
40. Zhao, X.; Ning, S.; Fu, W.; Pennycook, S.J.; Loh, K.P. Differentiating polymorphs in molybdenum disulfide via electron microscopy. *Adv. Mater.* **2018**, *30*, 1802397. [[CrossRef](#)]
41. Mishra, R.K.; Krishnaih, M.; Kim, S.Y.; Kushwaha, A.K.; Jin, S.H. Binder-free, scalable hierarchical MoS₂ as electrode materials in symmetric supercapacitors for energy harvesting applications. *Mat. Lett.* **2019**, *236*, 167–170. [[CrossRef](#)]
42. Mishra, R.K.; Kushwaha, A.K.; Kim, S.; Seo, S.G.; Jin, S.H. Vertical-slate-like MoS₂ nanostructures on 3D-Ni-foam for binder-free, low-cost, and scalable solid-state symmetric supercapacitors. *Curr. Appl. Phys.* **2019**, *19*, 1–7. [[CrossRef](#)]
43. Mishra, R.K.; Manivannan, S.; Kim, K.; Kwon, H.-I.; Jin, S.H. Petal-like MoS₂ nanostructures with metallic 1 T phase for high performance supercapacitors. *Curr. Appl. Phys.* **2018**, *18*, 345–352. [[CrossRef](#)]